Activation of The P62-Keap1-NRF2 Pathway Protects Against Ferroptosis in Radiation-Induced Lung Injury

Xuan Li
  Jinshan Hospital of Fudan University

Jingyao Chen
  Shanghai Medical University: Fudan University

Sujuan Yuan
  Jinshan Hospital of Fudan University

Xibing Zhuang
  Jinshan Hospital of Fudan University

Tiankui Qiao (✉ qiaotiankui@fudan.edu.cn)
  Tumor Diagnosis and Therapy, Jinshan Hospital, Fudan University   https://orcid.org/0000-0002-0454-0616

Abstract

Background

Radiation-induced lung injury (RILI) is one of the most common, serious and dose-limiting complications of thoracic radiotherapy. A primary reason for this is the radiation-induced cell death. Ferroptosis is a recently recognized form of regulated cell death, characterized by the accumulation of lipid peroxidation products and lethal reactive oxygen species (ROS). The ROS induced by irradiation might be the original trigger of ferroptosis in RILI. Furthermore, activation of the P62-Kelch-like ECH-associated protein 1 (Keap1)-nuclear factor erythroid 2-related factor 2 (NRF2) pathway has been shown to exert a protective effect, blunting ferroptosis. Therefore, this study aims to explore the protective effect of the P62-Keap1-NRF2 pathway against radiation-induced ferroptosis in alveolar epithelial cells.

Results

Firstly, our results demonstrated that radiation induced ferroptosis in vitro RILI cell model, which could be significantly reduced by Ferrostatin-1 (Fer-1), a specific inhibitor of ferroptosis. Then, we found that overexpression of P62 interacted with Keap1 to promote NRF2 translocation into the nucleus and upregulation its target proteins quinone oxidoreductase 1 (NQO1), heme oxygenase 1 (HO1) and ferritin heavy chain 1 (FTH1).

Conclusion

Collectively, the activation of the P62-Keap1-NRF2 pathway prevents radiation-induced ferroptosis in RILI cells, providing a theoretical basis for further research to find a potential approach for RILI therapy.

Background

Radiotherapy remains the primary modality in cancer treatment besides chemotherapy and surgery. However, radiation-induced lung injury (RILI), consisting of radiation-induced pneumonitis (RIP) and radiation-induced lung fibrosis (RILF), is a major and potentially life-threatening complication of thoracic radiotherapy[1]. It occurs in 5-20% of patients, severely limiting the curative effects of radiotherapy and degrading the quality of patients' life[2]. Currently, further understanding of the precise molecular mechanism of RILI has been an important step in developing new strategies to minimize radiation-induced injury.

More recently, ferroptosis has been identified as one of forms of regulated cell death (RCD) distinct from apoptosis, triggered by the accumulation of lipid peroxides as the lethal event due to decreased degradation by glutathione peroxidase[3, 4]. Ferroptosis has been implicated in multiple distinct diseases, including acute kidney injury, Parkinson's disease, carcinoma, stroke, intracerebral hemorrhage, traumatic

brain injury and ischemia-reperfusion injury[5–7]. Iron accumulation and lipid peroxidation are two key signals that initiate membrane oxidative damage during ferroptosis[8]. Abnormal iron metabolism, leading to ferroptosis, can occur through two major pathways. One is iron-mediated reactive oxygen species (ROS) production through the Fenton reaction and the other is involved in the activation of iron-containing enzymes[9].

P62 is a ubiquitin-binding autophagy receptor and signaling protein that can trigger a self-amplifying auto-regulatory loop that sustains the nuclear factor erythroid 2-related factor 2 (NRF2) activation[10]. NRF2 and the Kelch-like ECH-associated protein 1 (Keap1) are crucial regulators responsible for antioxidant response[11]. Keap1 is a cysteine-rich protein sensitive to modification by electrophiles and oxidants, which cause conformational changes of Keap1 that stabilize the Keap1-NRF2 interaction, preventing NRF2 proteasomal degradation[12]. NRF2 plays a critical role in attenuating inflammation and combating oxidative stress[13, 14].

Accumulating evidence has demonstrated that the generation of ROS caused by radiation is the primary mechanism contributing to radiation-induced lung injury and the activation of P62-Keap1-NRF2 pathway can inhibit the occurrence of ferroptosis[15]. Our previous study has suggested that ferroptosis played a central role in RILI in mice and NRF2 signaling pathway was involved in the regulation of ferroptosis[16]. Nonetheless, the underlying mechanism of ferroptosis in RILI including the interaction between ferroptosis-related genes has still not been studied profoundly.

Therefore, in this study, we designed a RILI cell model in which alveolar epithelial cells were exposed to 10Gy and explored the critical signal transduction pathways in the induction of ferroptosis in RILI. We demonstrated that oxidative stress caused by radiation activated the P62-Keap1-NRF2 pathway, inhibiting ferroptosis in the RILI cell model. Moreover, upregulation of NRF2 played a protective role in the RILI cells against ferroptosis through upregulation of multiple antioxidant proteins (quinone oxidoreductase 1 [NQO1], heme oxygenase 1 [HO1], and ferritin heavy chain 1 [FTH1]) involved in iron and ROS metabolism. Collectively, our results illustrated a novel therapeutic strategy to prevent and manage RILI.

Materials And Methods

Cell culture and reagent

The human NSCLC cell line A549 was obtained from the Cell Bank of the Chinese Academy of Sciences (Shanghai, China). Cells were maintained in RPMI-1640 medium (keygentec, China) containing 10% Fetal bovine serum (Cellsera, Australia), incubated at 37 °C in an environment of 5% CO_2 and 95% humidity. Ferrostatin-1 (MCE, USA), the first specific inhibitor of ferroptosis with obvious inhibition effect and great specificity, was prepared to the required concentration according to the product manual.

Experimental Design

A549 cells were randomly divided into ten groups with different treatments as follows: (1) control group; (2) irradiation (IR) group; (3) irradiation+Ferrostatin-1(IR+Fer-1) group; (4) IR+LV-NRF2 group; (5) IR+LV-p62 group; (6) IR+siRNA-Keap1 group; (7) LV-NRF2 group; (8) LV-P62 group; (9) siRNA-Keap1 group; (10) Ferrostatin-1(Fer-1) group. For irradiation, the cells were received 0, 2, 4, 6, 8, and 10 Gy X-ray radiation. The beam was 6 MV X-ray at a dose rate of 2.0 Gy/min. Cells were treated with different concentration of Ferrostatin-1 30 min before radiation in IR+Fer-1 group.

Clonogenic assay

For standard clonogenic assays, A549 cells were seeded into 6-well plates at density of 2000 cells per well and incubated for 24h. Then, the cells were pretreated with Fer-1 for 30 min, followed by 0, 2, 4, 6, 8, and 10 Gy X-ray radiation. The cells were incubated at 37 °C for another 12 days to allow for colony formation and subsequently stained with crystal violet. Only viable colonies consisting of 50 or more cells were counted.

Cell viability assay

A549 cells were plated at the density of 5×10^3 cells per well in 96-well plates. After overnight culture, cells were pretreated with various concentrations of Fer-1 for 30 min, followed by 0, 2, 4, 6, 8, and 10 Gy X-ray radiation. Cell viability was evaluated with Cell Counting Kit-8 Assay Kit (Do Jindo Laboratories, Kumamoto, Japan) according the manufacturer's instructions.

Quantitative real time polymerase chain reaction

Total RNA isolation was carried out by using the RNA Purification Kit (Yi Shan Biotechnology Company, Shanghai, China). The complementary DNA (cDNA) was synthesized and amplified with the reverse transcription kit (Takara, Osaka, Japan). cDNA from various cell samples was prepared by quantitative real time PCR kit (Takara, Osaka, Japan) with GAPDH as internal control and was amplified with specific primers (NRF2: forward 5'-TCTGCCAACTACTCCCAGGT-3' and reverse 5'- AATGTCTGCGCCAAAAGCTG -3'; P62: forward 5'-CCCTCTCCCAGATGCTGTCCAT-3' and reverse 5'-G CCGCTCCGAT GTCATAGTTCT-3'; Keap1: forward 5'-CGTGGCTGTCCTCAATCGTCTC-3' and reverse 5'-CGCTTCGGATGGTGTTCATTGC-3'; GAPDH: forward 5'-CAAATTCCATGGCACCGTCA-3' and reverse 5'-AGCATCGCCCCACTTGATTT-3').

Western blot analysis

Cells were lysed in RIPA buffer containing 1nM phenylmethylsulfonyl fluoride (PMSF) and phosphatase and protease inhibitors on ice. Then, the lysates were centrifuged at 12,000 g for 20 min at 4°C, and the protein concentration of the supernatant was determined using the BCA Protein Assay Kit (Thermo Scientific, USA). Equal amounts of protein were separated via 8% to 10% SDS-PAGE and transferred to polyvinylidene fluoride (PVDF) membranes (Millipore, Bedford, MA, USA). Next, the membranes were blocked with 5% skim milk for 1 h at room temperature and incubated with the desired primary antibodies overnight at 4°C, followed by incubation with horseradish peroxidase-coupled secondary antibodies. The

details of primary antibodies used in this paper were shown as follows: P62 (1:10000, ab155282, Abcam, UK), Keap1 (1:500, 10503-2-AP, Sanying BioTECH, China), Nrf2 (1:1000, ab62352, Abcam, UK), HO1 (1:500, 10701-1-AP, Sanying BioTECH, China), NQO1 ((1:500, 11451-1-AP, Sanying BioTECH, China), FTH1 (1:1000, ab170888, Abcam, UK) and rabbit anti-GAPDH (KGAA002, KeyGEN BioTECH, China, 1:10000). The immunocomplexes were finally analyzed using a chemiluminescence reagent (Millipore, Bedford, MA, USA) and detected on photographic film.

Morphological Observation of Mitochondria and Mitochondrial Membrane Potential Assay

The mitochondria morphology of A549 cells was observed by transmission electron microscopy (TEM). A549 cells were fixed with 2.5% glutaraldehyde in phosphoric acid buffer, post fixed in 1% osmium acid for 2h at room temperature, and dehydrated in a graded series of ethanol. The ultrathin sections were cut with a diamond knife and stained with 3% uranium acetate and lead citrate. Captured the TEM images using transmission electron microscope (JEM-1011, Japan).

Mitochondrial membrane potential was measured using Mitochondrial membrane potential assay kit with JC-1 (Keygen Biotech, Nanjing, China) according to the manufacturer's instructions. Briefly, cells were stained with JC-1 working solution for 20 min at 37 °C, washed twice with incubation buffer, and then analyzed by flow cytometry (Becton-Dickinson, USA).

Measurement of intracellular Fe^{2+} and ROS

The intracellular Fe^{2+} was determined using the fluorescent indicator PGSK (Keygen Biotech, Nanjing, China). Cell suspensions were collected and supplemented with the PGSK probe. After 30 min of incubation, cells were centrifuged, washed, and resuspended. Finally, the relative PGSK level was measured by flow cytometry (Becton-Dickinson, USA).

The ROS level was detected with the fluorescent probe DCFH-DA (Keygen Biotech, Nanjing, China) by flow cytometry. In brief, A549 cells with different treatments were incubated with DCFH-DA for 30 min at 37°C and subsequently washed with PBS. After incubation, the fluorescence of the cells was measured using flow cytometry (Becton-Dickinson, USA).

Measurement of lipid peroxidation and glutathione

MDA content, a product of lipid peroxidation, was used to assess the level of lipid peroxidation. The relative malondialdehyde (MDA) concentration in cell lysates was assessed using a Lipid Peroxidation (MDA) Assay Kit according the manufacturer's instructions. Briefly, the MDA in the sample reacts with thiobarbituric acid (TBA) to generate a MDA-TBA adduct. The MDA-TBA adduct can be easily quantified colorimetrically (OD = 532 nm). Values were normalized for protein content of the lysates. The relative glutathione (GSH) concentration in cell lysates was estimated using a Glutathione Assay Kit according the manufacturer's instructions.

Immunofluorescence

After treatment, cells were plated on glass coverslips and fixed with 4% paraformaldehyde for 15 minutes and then blocked with 5% BSA for 1 hour at room temperature. Immunofluorescence was performed by incubating with antibodies against GPX4 (1:200, ab125066, Abcam, UK) and ACSL4 (1:100, ab155282, Abcam, UK) at 4 °C overnight. On the second day, cells were incubated with Goat Anti-Rabbit IgG antibodies and then washed thrice in PBS. Nuclei were counterstained using 4□,6-diamidino-2-phenylindole (DAPI) for 10 minutes. The cells were observed under a fluorescence microscope.

Statistical analysis

Statistical analysis was performed through GraphPad Prism 7 (GraphPad Software, San Diego, CA, USA). Results were presented as the mean ± SD. The differences between pairwise comparisons were determined using Student's t-test. The comparisons among multiple groups were carried out by one-way ANOVA followed by a Bonferroni correction. Various of P less than 0.05 were considered statistically significant.

Results

Radiation induced ferroptosis in A549 cells

To establish RILI cell model, we selected A549 cells as the experimental object. Through different doses of radiation intervention and cell proliferation activity detected by cell clone formation and CCK-8 experiments, the clone number and the cell viabilities of A549 cells decreased in a dose-dependent manner (Fig. 1). Treated with 10Gy X-ray, the inhibition rate of cells 24h after irradiation (56.7%) was the closest to the fifty percent inhibitory concentration (IC50). Therefore, 10Gy 6 MV X-ray and detect RILI related indexes 24 hours after irradiation as the best model to establish RILI cell model.

According to the results of the cell clone formation and CCK-8 tests (Fig. 2), various concentrations (0.1, 0.5, 1, 5uM) of Fer-1 had no significant cytotoxic effects on A549 cells. Next, we administrated RILI cells with Fer-1 at concentrations of 0.1, 0.5 and 1uM and found that with the increase in the concentration, the cell clone number increased and the cell inhibition rate decreased. Collectively, these data indicated that Fer-1 could suppress radiation-mediated ferroptosis in a dose-dependent manner in RILI cells and 1uM was selected as effective dose in the follow-up study.

Ferroptosis inhibitor exerted a protective effect in ferroptosis in RILI cells

Available evidences have demonstrated that ferroptosis is characterized by redox imbalance and the impairment of lipid metabolism[17, 18]. To further verify the availability of RILI cell model and the role of ferroptosis in RILI, the intracellular Fe^{2+} was determined using the fluorescent indicator PGSK (Fig. 3). Compared with control group, Fe^{2+} was found to be dramatically reduced in IR group, whereas Fer-1 significantly reversed the decrease of Fe^{2+}. Overexpression of P62 or NRF2 had the same protective effect as Fer-1.

The abnormal increase of ROS tends to reflect the occurrence of RILI[2]. Next, the ROS level was detected using the fluorescent probe DCFH-DA by flow cytometry. As shown in Fig. 4, the ROS level after radiation was obviously higher than that without radiation. Likewise, Fer-1, silencing Keap1 or overexpression of P62 or NRF2 improved the ROS level, approving that ferroptosis contributed to radiation-induced lung injury.

The increased oxidative stress induced by redox imbalance can generate a variety of lipid peroxidation products or might involve in alterations in lipid metabolism[19]. Oxidative stress was assessed by evaluating contents of MDA and GSH. The data (Fig. 5) exhibited that the irradiation group displayed elevated contents of MDA and decreased level of GSH, while Fer-1, silencing Keap1 or overexpression of P62 or NRF2 suppressed the increase of GSH depletion and contents of MDA remarkably.

Overall, ferroptosis inhibitor protects RILI cells from redox imbalance and the impairment of lipid metabolism and P62-Keap1-NRF2 pathway regulated the process of ferroptosis in RILI.

Ferroptosis inhibitor protected mitochondrial membrane from radiation-induced injury

Previous findings have showed that the decline of mitochondrial membrane potential, the obvious shrinkage of mitochondrial morphology and the increase of membrane density are typical features of ferroptosis[20, 21]. The results of the TEM illustrated that radiation led to decreased volume of mitochondria and increase of mitochondrial membrane density[22]. Compared with IR group, the volume of mitochondria decreased and the membrane density increased in IR+Fer-1 group, IR+LV-NRF2 group, IR+LV-P62 group and IR+siRNA-Keap1 group (Fig. 6 A). Next, JC-1 fluorescent probe was used to detect mitochondrial membrane potential by flow cytometry (Fig. 6 B). The mitochondrial of RILI cells were significantly depolarized. Fer-1 could ameliorate mitochondrial depolarization, further indicating the involvement of ferroptosis in RILI. Likewise, silencing Keap1 or overexpressing P62 or NRF2 had the same effect, keeping decreased mitochondrial membrane potential.

P62-Keap1-NRF2 pathway had been activated in ferroptosis in RILI cells

To determine the underlying mechanism of ferroptosis in RILI, we analyzed the activation of ferroptosis markers by immunofluorescence (Fig. 7). The results showed that IR group significantly decreased the expression of GPX4, the key regulator enzyme of ferroptosis, but increased the expression of ACSL4, another pivotal factor determining the sensitivity of ferroptosis.

Several studies have demonstrated that P62-Keap1-NRF2 pathway was involved in the regulation of ferroptosis[22, 23]. To further explore the role of P62-Keap1-NRF2 pathway in RILI cells, siRNA Keap1, LV-P62 and LV-NRF2 were transfected to achieve Keap1 silencing and P62 and NRF2 overexpressing. Subsequently, quantitative real-time PCR was performed to verify the transfection efficiency, suggesting that the mRNA expression of P62 and NRF2 increased significantly compared with the control and the LV-control groups. Western blotting and quantitative real-time PCR revealed that overexpressing P62 significantly suppressed the levels of Keap1 but elevated the expression of NRF2 (Fig. 8). However,

overexpressing NRF2 or silencing Keap1 didn't exerts influence to the expression of P62, indicating that Keap1 and NRF2 were located downstream of P62. Down-regulation of Keap1 expression could promote NRF2 expression into nucleus. The downstream antioxidant proteins such as HO1, FTH1 and NQO1 were also detected. Up-regulation P62 or NRF2 facilitated the expression of antioxidative protein such as HO1, FTH1 and NQO1. Fer-1 intervention didn't induce P62 protein and mRNA expression in RILI cells while remarkably induced Keap1 protein expression, but not its mRNA level. The levels of NRF2 protein and mRNA increased significantly as well as the levels of antioxidant protein HO1, FTH1 and NQO1. Taken together, P62-Keap1-NRF2 pathway was responsible for the process of ferroptosis in RILI.

Discussion

Cell death is one of the critical pathophysiological processes in the occurrence and development of RILI[24]. The death of alveolar epithelial cells will destroy the integrity of alveolar respiratory membrane, resulting in the failure of pulmonary surfactant, collapse of alveoli, followed by pulmonary edema, and finally the occurrence of RILI[1, 25]. Therefore, it is representative to the construction of RILI cell model with alveolar epithelial cells. In our study, A549 cells were selected as the experimental object. Through different doses of radiation intervention and cell proliferation activity detected by cell clone formation and CCK-8 experiments, we found that 10Gy 6 MV X-ray and detect RILI related indexes 24 hours after irradiation as the best model to establish RILI cell model. Fer-1 was the first specific inhibitor of ferroptosis with obvious inhibition effect and great specificity, widely administrated in ferroptosis-related experiments[8, 26]. Through cell clone formation and CCK-8 experiments, we selected Fer-1 1um as an effective dose to inhibit the ferroptosis of RILI cells, which was consistent with the effective dose inhibiting ferroptosis in a variety of peroxidation diseases[27, 28].

To further verify the availability of RILI cell model and the role of ferroptosis in RILI, we intervened RILI cells with Ferrostatin-1 and then detected the related indicators of RILI and ferroptosis. Our findings demonstrated that the level of ROS and MDA in RILI cells increased significantly, and the levels of GSH decreased remarkably, which suggested that RILI cell model was successfully established. Furthermore, the reduction of ROS and MDA levels and the increase of GSH levels indirectly indicated the occurrence of ferroptosis in RILI.

The decline of mitochondrial membrane potential, the obvious shrinkage of mitochondrial morphology and the increase of membrane density are typical features of ferroptosis, as well as the direct morphological evidence for detecting the occurrence of ferroptosis[29]. The metabolism disorder of iron ions disturbed by intracellular peroxidation, and the decrease of Fe^{2+} level are the metabolic characteristics of ferroptosis[8]. GPX4 is the key regulator enzyme of ferroptosis, and its expression level is usually used as an indicator of ferroptosis[30]. ACSL4 is also another pivotal factor determining the sensitivity of ferroptosis in cells by enriching ω6 Fatty acids and the increase of its expression level can also be used as a marker of ferroptosis[31, 32]. In this study, under electron microscopy, the mitochondrial morphology shrunk, the membrane density thickened, the level of Fe^{2+} and GPX4 decreased considerably

and the expression level of ACSL4 increased in RILI cells. With the intervention of Fer-1, the state of mitochondria, iron metabolism, GPX4 and ACSL4 expression in RILI cells were improved.

NRF2 signaling pathway plays a paramount role not only in antioxidation in RILI, but also in regulating the occurrence of ferroptosis[33, 34]. Studies have found that activation of P62-Keap1-NRF2 pathway can inhibit the occurrence of ferroptosis[22, 23]. In our previous study, we found that NRF2 pathway was involved in the regulation of ferroptosis in RILI, but the specific regulatory mechanism and the regulatory relationship of each part remained unclear.

P62 is a key molecule that regulates the function of various intracellular signaling pathways and participates in the regulation of apoptosis, autophagy and other functions[35]. P62 can activate the expression of Keap1-NRF2 signaling pathway, while NRF2 can activate the expression of NRF2 in a positive feedback loop, and P62-NRF2 pathway can be activated even without the modification of Keap1[36–38]. NRF2 plays a central role in the regulation of endogenous antioxidant response. During cell peroxidation, the expression of Keap1 in the cytoplasm was inhibited, and NRF2-Keap1 was dissociated, which promoted NRF2 to enter the nucleus, up-regulated the production of antioxidant protein, and ultimately reduced the level of ROS and oxidative stress injury[39, 40].

NRF2 was degraded by Keap1 continuously, therefore down-regulation of Keap1 expression could promote NRF2 expression into nucleus and up-regulate the level of antioxidant protein[41]. P62-Keap1-NRF2 signaling pathway negatively regulated the occurrence of ferroptosis in hepatoma cells. Knockdown of P62 expression resulted in up-regulation of Keap1 expression, which enhanced the degradation of NRF2 mediated by Keap1, decreased the entry of NRF2 into the nucleus, and decreased the antioxidant proteins caused by inhibition of NRF2 signaling pathway, such as HO1, FTH1 and NQO1, enhancing the sensitivity of drug-induced ferroptosis in hepatoma cells[23].

In this study, we demonstrated that the expression of P62 and NRF2, as well as the levels of HO1, FTH1 and NQO1 in RILI cells, were upregulated, and Keap1 was downregulated, whereas the overall change was inconspicuous. This may be due to the activation of endogenous P62-Keap1-NRF2 signaling pathway to keep the stabilization of redox balanced in RILI cells in response to the peroxide state. Furthermore, Fer-1 intervention didn't induce P62 protein and mRNA expression in RILI cells while remarkably induced Keap1 protein expression, but not its mRNA level. The levels of NRF2 protein and mRNA increased significantly as well as the levels of antioxidant protein HO1, FTH1 and NQO1. Collectively, these findings suggest that Fer-1 can further activate NRF2 signaling pathway, increase antioxidant protein, reduce ROS production thus inhibiting ferroptosis. NRF2 may be the site of action of Fer-1, not P62 and Keap1. The decrease of transcription-dependent of Keap1 may be caused by the activation of NRF2 expression by Fer-1, the enhancement of Keap1-NRF2 complex and the continuous degradation of Keap1.

To further explore the specific role of P62-Keap1-NRF2 in the regulation of ferroptosis in RILI cells, we constructed P62 and NRF2 overexpression plasmids and Keap1 siRNA into RILI cells. The results showed that up-regulation of P62 contributed to down-regulation of Keap1 and promoted NRF2 to transfer into nucleus, thus the levels of antioxidant proteins HO1, FTH1 and NQO1 in RILI cells as well as GSH and

Fe^{2+} were increased while the levels of ROS and MDA were decreased. Moreover, the number of intracellular shrinkage and membrane low potential mitochondria was decreased, the level of GPX4 was increased, and the level of ACSI4 was decreased, indicating that the intracellular ferroptosis was inhibited. These results jointly further confirmed the inhibition of ferroptosis in RILI by activating P62-Keap1-NRF2 signaling pathway.

Conclusions

In summary, we successfully established the RILI cell model and demonstrated a form of regulated cell death, ferroptosis, caused by irradiation, which was distinct from the classical cell apoptosis. The beneficial effect of ferroptosis interference opened a new pathway to reduce ROS damage and protect against the RILI. In RILI, as shown in Fig. 9, a large number of ROS were produced by radiation ionization. The cells were in the state of oxidative stress, which activated the endogenous P62-Keap1-NRF2 antioxidant signaling pathway, but the increase of NRF2 expression level was limited. Fer-1 can activate NRF2 signaling pathway in RILI, up-regulating the expression of antioxidant proteins, reducing the production of ROS and blocking the occurrence of ferroptosis. P62-Keap1-NRF2 signaling pathway is involved in the regulation of ferroptosis in RILI. By activating the expression of P62, Keap1 expression was blocked, which transformed NRF2 into nuclear for expression, and NRF2 antioxidant signaling pathway is activated, which increased antioxidant protein production and reduced the ROS level, and finally inhibited ferroptosis. Thus, P62-Keap1-NRF2 signaling pathway activation represents a potential new therapeutic approach to prevent RILI.

Abbreviations

RILI, radiation- induced lung injury; RIP, radiation-induced pneumonitis; RILF, radiation-induced lung fibrosis; RCD, regulated cell death; ROS, reactive oxygen species; Keap1, kelch-like ECH-associated protein 1; NRF2, nuclear factor erythroid 2-related factor 2; Fer-1, ferrostatin-1; HO1, heme oxygenase 1; NQO1, quinone oxidoreductase 1; FTH1, ferritin heavy chain 1; PMSF, phenylmethylsulfonyl fluoride; PVDF, polyvinylidene fluoride; TEM, transmission electron microscopy; MDA, malondialdehyde; GSH, glutathione; GPX4, glutathione peroxidase 4; ACSL4, acyl-CoA synthetase long chain family member 4; IR, ionizing radiation.

Declarations

Acknowledgements

Not applicable.

Funding

201409001100]. This work was supported by these two grants.

Ethics approval

Compliance with Ethical Standards.

Competing interests

The authors declare that they have no conflict of interest.

Consent for publication

Not applicable.

Availability of data and material

All data generated or analyzed during this study are included in this published article.

Code availability

Not applicable.

Author information

Affiliations

Jinshan Hospital Center for Tumor Diagnosis & Therapy, Jinshan Hospital, Fudan University Shanghai Medical School, Shanghai 201508, China.

Xuan Li, Sujuan Yuan, Xibing Zhuang & Tiankui Qiao.

Fudan University Shanghai Medical School, Shanghai 200032, China.

Jingyao Chen.

Contributions

Tiankui Qiao and Xuan Li contributed to the study conception and design. Material preparation, data collection and analysis were performed by Xuan Li, Sujuan Yuan and Xibing Zhuang. The first draft of the manuscript was written by Jingyao Chen and all authors commented on previous versions of the manuscript. All authors read and approved the final manuscript.

References

1. Käsmann, L., et al., *Radiation-induced lung toxicity - cellular and molecular mechanisms of pathogenesis, management, and literature review*. Radiat Oncol, 2020. **15**(1): p. 214.

2. Giuranno, L., et al., *Radiation-Induced Lung Injury (RILI)*. Front Oncol, 2019. **9**: p. 877.

3. Lei, P., T. Bai, and Y. Sun, *Mechanisms of Ferroptosis and Relations With Regulated Cell Death: A Review.* Front Physiol, 2019. **10**: p. 139.

4. Lang, X., et al., *Radiotherapy and Immunotherapy Promote Tumoral Lipid Oxidation and Ferroptosis via Synergistic Repression of SLC7A11*. Cancer Discov, 2019. **9**(12): p. 1673–1685.

5. Stockwell, B.R., et al., *Ferroptosis: A Regulated Cell Death Nexus Linking Metabolism, Redox Biology, and Disease*. Cell, 2017. **171**(2): p. 273–285.

6. Sun, Y., et al., *Activation of p62-Keap1-Nrf2 Pathway Protects 6-Hydroxydopamine-Induced Ferroptosis in Dopaminergic Cells*. Mol Neurobiol, 2020. **57**(11): p. 4628–4641.

7. Wang, Y., et al., *Quercetin alleviates acute kidney injury by inhibiting ferroptosis*. J Adv Res, 2021. **28**: p. 231–243.

8. Dixon, S.J., et al., *Ferroptosis: an iron-dependent form of nonapoptotic cell death*. Cell, 2012. **149**(5): p. 1060–72.

9. Li, C., et al., *Mitochondrial DNA stress triggers autophagy-dependent ferroptotic death*. Autophagy, 2021. **17**(4): p. 948–960.

10. Umemura, A., et al., *p62, Upregulated during Preneoplasia, Induces Hepatocellular Carcinogenesis by Maintaining Survival of Stressed HCC-Initiating Cells*. Cancer Cell, 2016. **29**(6): p. 935–948.

11. Ma, Q., *Role of nrf2 in oxidative stress and toxicity*. Annu Rev Pharmacol Toxicol, 2013. **53**: p. 401–26.

12. Gallego-Selles, A., et al., *Regulation of Nrf2/Keap1 signalling in human skeletal muscle during exercise to exhaustion in normoxia, severe acute hypoxia and post-exercise ischaemia: Influence of metabolite accumulation and oxygenation*. Redox Biol, 2020. **36**: p. 101627.

13. Sun, X., et al., *Octyl itaconate inhibits osteoclastogenesis by suppressing Hrd1 and activating Nrf2 signaling*. Faseb j, 2019. **33**(11): p. 12929–12940.

14. Chan, K., X.D. Han, and Y.W. Kan, *An important function of Nrf2 in combating oxidative stress: detoxification of acetaminophen*. Proc Natl Acad Sci U S A, 2001. **98**(8): p. 4611–6.

15. Azzam, E.I., J.P. Jay-Gerin, and D. Pain, *Ionizing radiation-induced metabolic oxidative stress and prolonged cell injury*. Cancer Lett, 2012. **327**(1-2): p. 48–60.

16. Li, X., et al., *Ferroptosis inhibitor alleviates Radiation-induced lung fibrosis (RILF) via down-regulation of TGF-β1*. J Inflamm (Lond), 2019. **16**: p. 11.

17. Hirschhorn, T. and B.R. Stockwell, *The development of the concept of ferroptosis*. Free Radic Biol Med, 2019. **133**: p. 130–143.

18. Stockwell, B.R., X. Jiang, and W. Gu, *Emerging Mechanisms and Disease Relevance of Ferroptosis*. Trends Cell Biol, 2020. **30**(6): p. 478–490.

19. Hu, C., M. Wang, and X. Han, *Shotgun lipidomics in substantiating lipid peroxidation in redox biology: Methods and applications*. Redox Biol, 2017. **12**: p. 946–955.

20. Wang, H., et al., *Mitochondria regulation in ferroptosis*. Eur J Cell Biol, 2020. **99**(1): p. 151058.

21. Wu, H., et al., *The Multifaceted Regulation of Mitochondria in Ferroptosis*. Life (Basel), 2021. **11**(3).

22. Xie, Y., et al., *Ferroptosis: process and function*. Cell Death Differ, 2016. **23**(3): p. 369–79.

23. Sun, X., et al., *Activation of the p62-Keap1-NRF2 pathway protects against ferroptosis in hepatocellular carcinoma cells*. Hepatology, 2016. **63**(1): p. 173–84.

24. Sia, J., et al., *Molecular Mechanisms of Radiation-Induced Cancer Cell Death: A Primer*. Front Cell Dev Biol, 2020. **8**: p. 41.

25. Han, S. and R.K. Mallampalli, *The acute respiratory distress syndrome: from mechanism to translation*. J Immunol, 2015. **194**(3): p. 855–60.

26. Kabiraj, P., et al., *The neuroprotective role of ferrostatin-1 under rotenone-induced oxidative stress in dopaminergic neuroblastoma cells*. Protein J, 2015. **34**(5): p. 349–58.

27. Liu, P., et al., *Ferroptosis contributes to isoflurane-induced neurotoxicity and learning and memory impairment*. Cell Death Discov, 2021. **7**(1): p. 72.

28. Wu, C., et al., *Induction of ferroptosis and mitochondrial dysfunction by oxidative stress in PC12 cells*. Sci Rep, 2018. **8**(1): p. 574.

29. Jelinek, A., et al., *Mitochondrial rescue prevents glutathione peroxidase-dependent ferroptosis*. Free Radic Biol Med, 2018. **117**: p. 45–57.

30. Chen, X., et al., *Cellular degradation systems in ferroptosis*. Cell Death Differ, 2021. **28**(4): p. 1135–1148.

31. Cui, Y., et al., *ACSL4 exacerbates ischemic stroke by promoting ferroptosis-induced brain injury and neuroinflammation*. Brain Behav Immun, 2021. **93**: p. 312–321.

32. Li, Y., et al., *Ischemia-induced ACSL4 activation contributes to ferroptosis-mediated tissue injury in intestinal ischemia/reperfusion*. Cell Death Differ, 2019. **26**(11): p. 2284–2299.

33. Cameron, B.D., et al., *The Role of Nrf2 in the Response to Normal Tissue Radiation Injury*. Radiat Res, 2018. **190**(2): p. 99–106.

34. Traver, G., et al., *Loss of Nrf2 promotes alveolar type 2 cell loss in irradiated, fibrotic lung*. Free Radic Biol Med, 2017. **112**: p. 578–586.

35. Moscat, J. and M.T. Diaz-Meco, *p62 at the crossroads of autophagy, apoptosis, and cancer*. Cell, 2009. **137**(6): p. 1001-4.

36. Ichimura, Y. and M. Komatsu, *Activation of p62/SQSTM1-Keap1-Nuclear Factor Erythroid 2-Related Factor 2 Pathway in Cancer*. Front Oncol, 2018. **8**: p. 210.

37. Komatsu, M., et al., *The selective autophagy substrate p62 activates the stress responsive transcription factor Nrf2 through inactivation of Keap1*. Nat Cell Biol, 2010. **12**(3): p. 213–23.

38. Jain, A., et al., *p62/SQSTM1 is a target gene for transcription factor NRF2 and creates a positive feedback loop by inducing antioxidant response element-driven gene transcription*. J Biol Chem, 2010. **285**(29): p. 22576-91.

39. Kang, M.I., et al., *Scaffolding of Keap1 to the actin cytoskeleton controls the function of Nrf2 as key regulator of cytoprotective phase 2 genes*. Proc Natl Acad Sci U S A, 2004. **101**(7): p. 2046–51.

40. Velichkova, M. and T. Hasson, *Keap1 regulates the oxidation-sensitive shuttling of Nrf2 into and out of the nucleus via a Crm1-dependent nuclear export mechanism*. Mol Cell Biol, 2005. **25**(11): p. 4501–13.

41. Kobayashi, A., et al., *Oxidative and electrophilic stresses activate Nrf2 through inhibition of ubiquitination activity of Keap1*. Mol Cell Biol, 2006. **26**(1): p. 221–9.
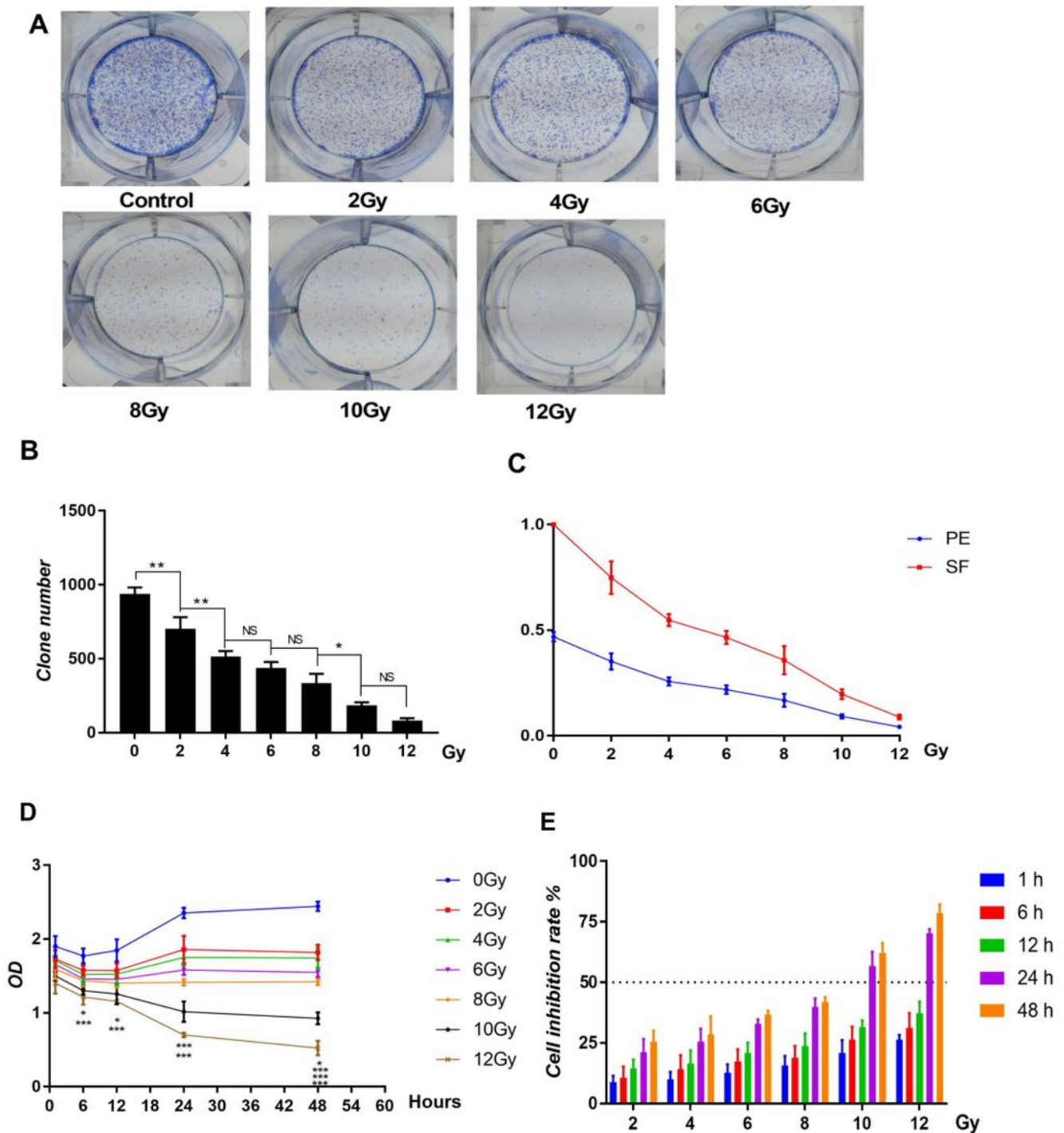
Figures

Figure 1

RILI cell model. A, B Changes of colony formation number of A549 cells in six well plate under different radiation doses. C Cell clone formation rate (PE) and cell survival fraction (SF) under different radiation doses. D OD values at different time points after irradiation in different radiation dose groups with CCK-8. E Cell inhibition rate in different dose groups at different time points after irradiation. (Data shown as

mean ± SD, one-way ANOVA followed by a Bonferroni correction, NS Represented no statistical difference. * P ⩽ 0.05, ** P ⩽ 0.01, *** P ⩽0.001).
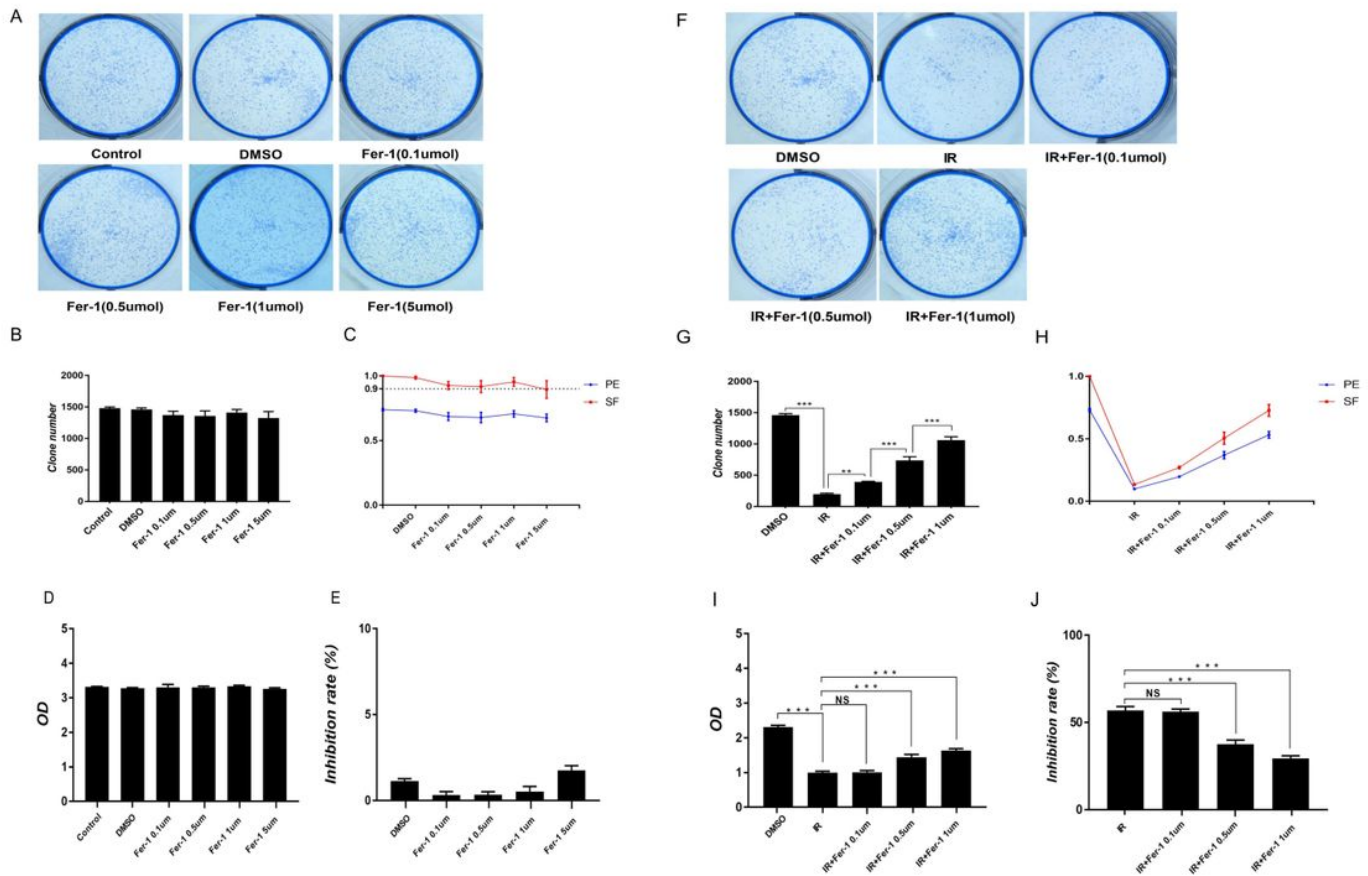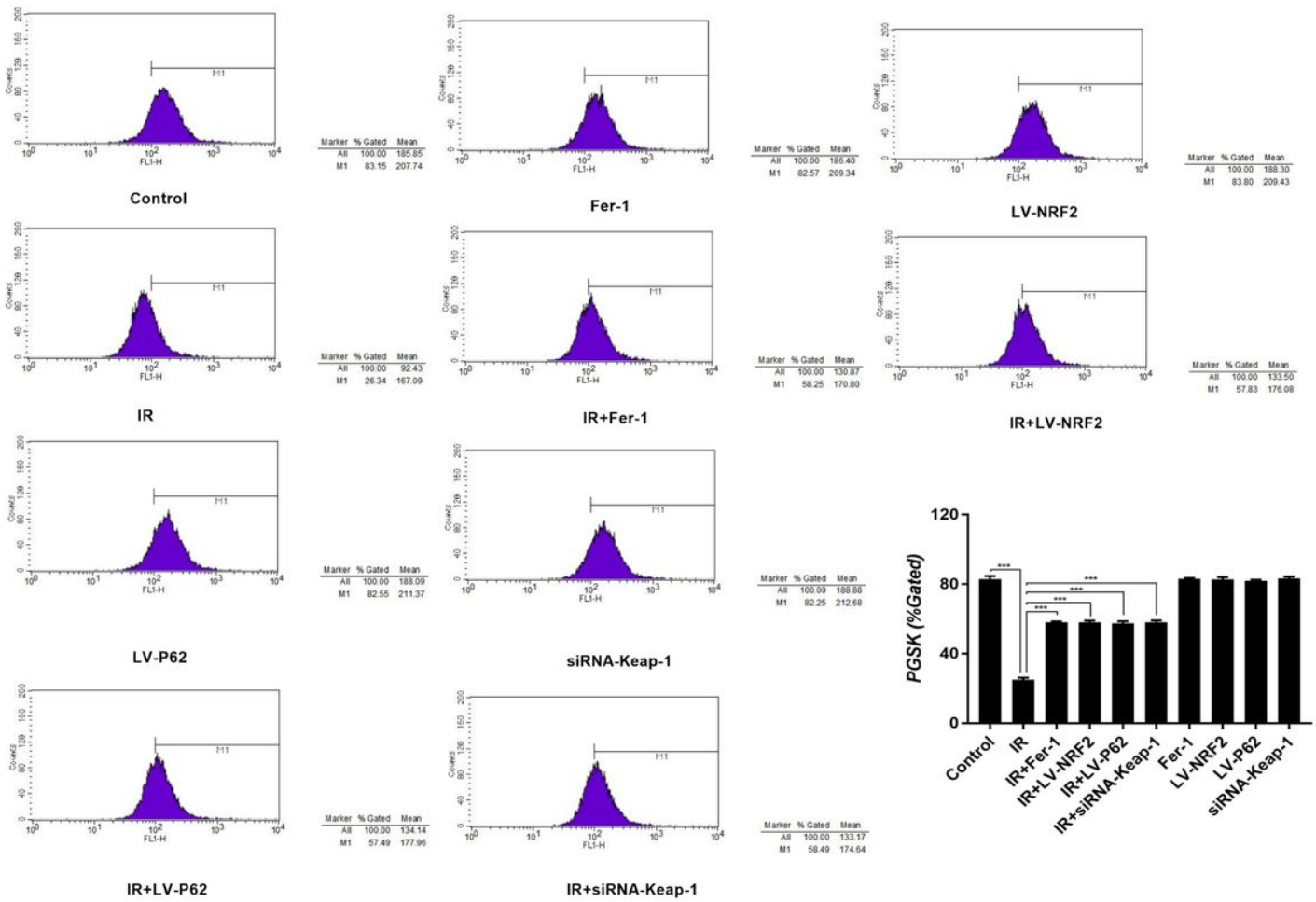

Figure 2

Cytotoxicity and effective concentration selection of Fer-1 on RILI cell. A, B Changes of colony formation number of A549 cells in six well plate under different concentrations of Fer-1. C A549 cells clone formation rate (PE) and cell survival fraction (SF) under different concentrations of Fer-1. D, E OD values and cell inhibition rate of A549 cells in different concentrations of Fer-1 with CCK-8. F, G Changes of colony formation number of RILI cells in six well plate under different concentrations of Fer-1. H RILI cells clone formation rate (PE) and cell survival fraction (SF) under different concentrations of Fer-1. I, J OD values and cell inhibition rate of RILI cells in different concentrations of Fer-1 with CCK-8. (Data shown as mean ± SD, one-way ANOVA followed by a Bonferroni correction, NS Represented no statistical difference. * P ⩽ 0.05, ** P ⩽ 0.01, *** P ⩽0.001).

Figure 3

The intracellular Fe2+ with the fluorescent indicator PGSK. (Data shown as mean ± SD, one-way ANOVA followed by a Bonferroni correction, *** P ⬚0.001).
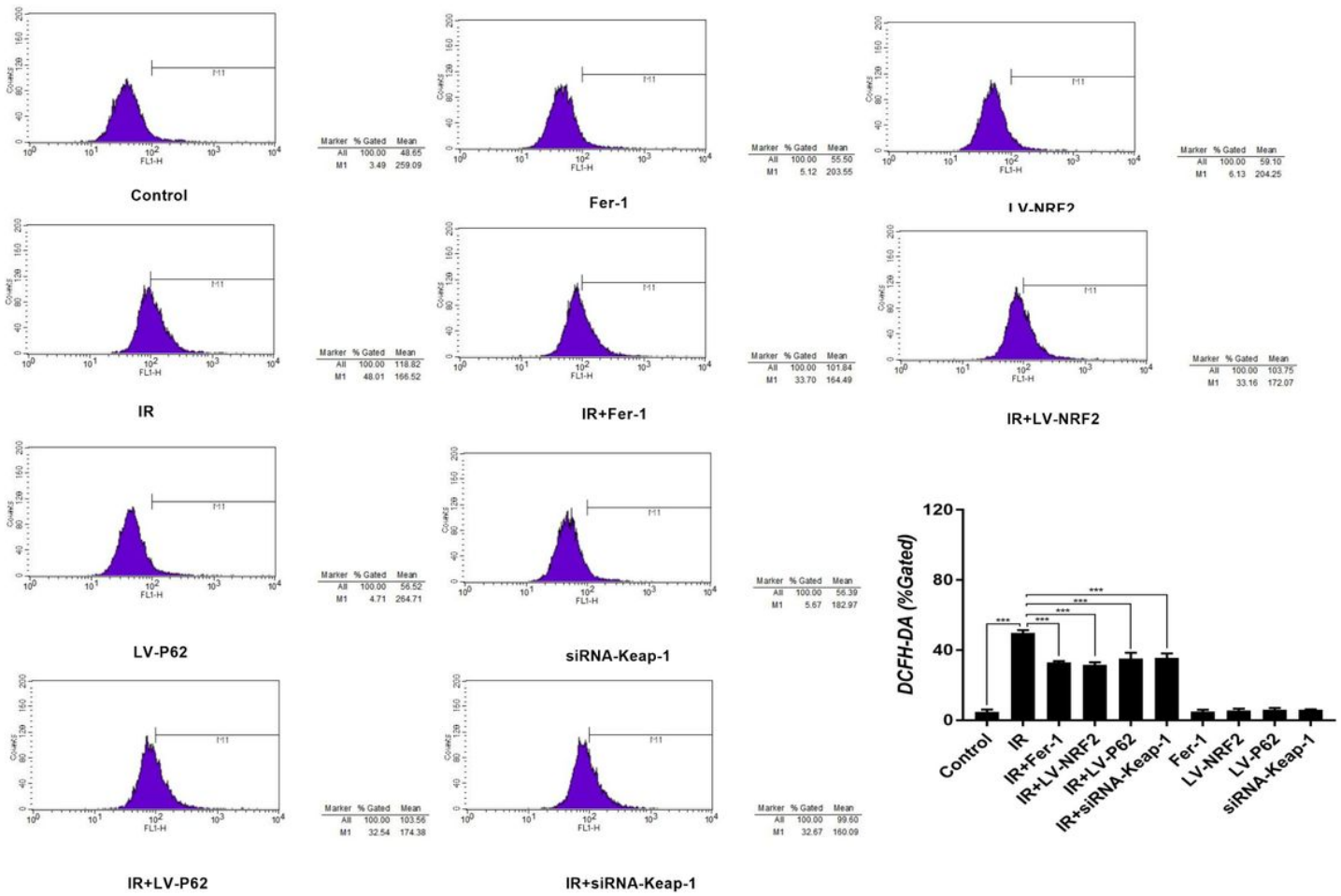
Figure 4

The ROS levels with the fluorescent probe DCFH-DA. (Data shown as mean ± SD, one-way ANOVA followed by a Bonferroni correction, *** P ⩽ 0.001).
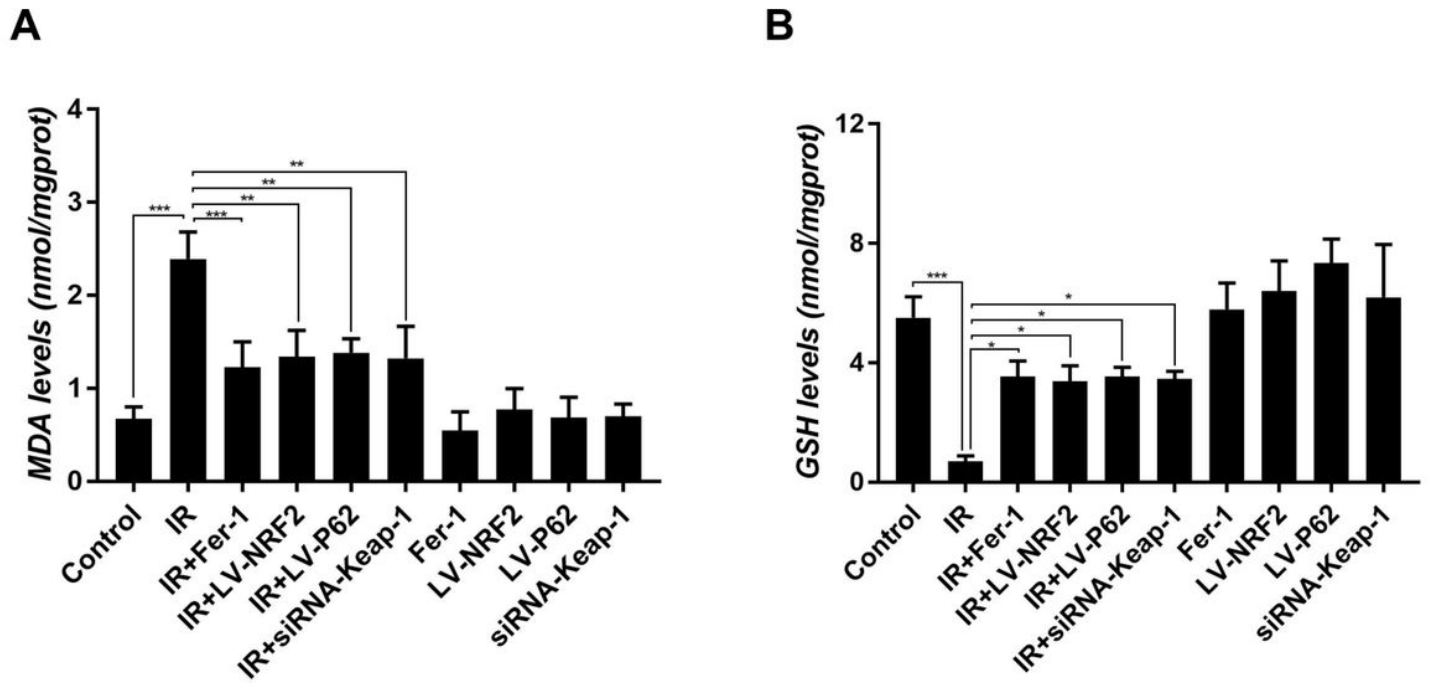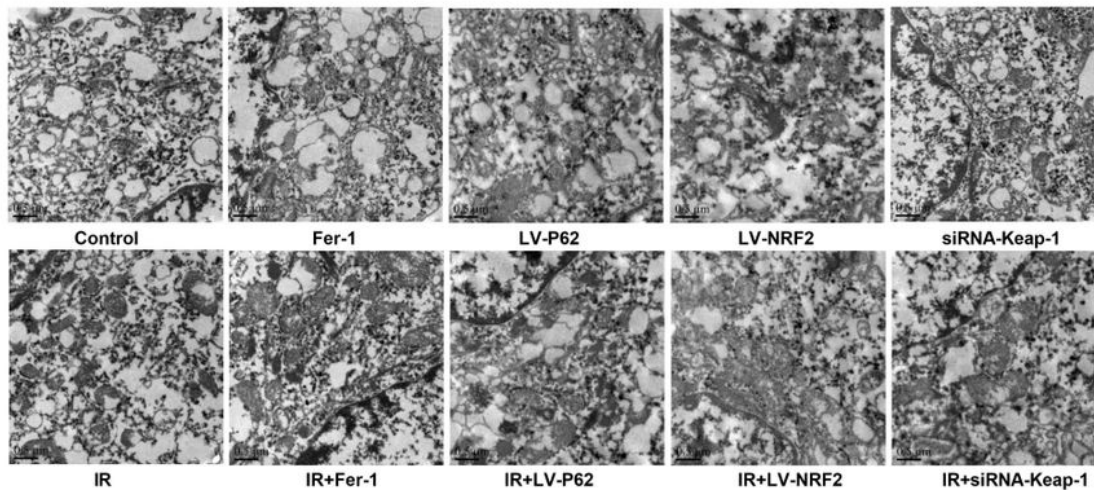
Figure 5

Measurement of lipid peroxidation and glutathione. A, B MDA and GSH levels of each group. (Data shown as mean ± SD, one-way ANOVA followed by a Bonferroni correction, * P ⬚ 0.05, ** P ⬚ 0.01, *** P ⬚0.001).
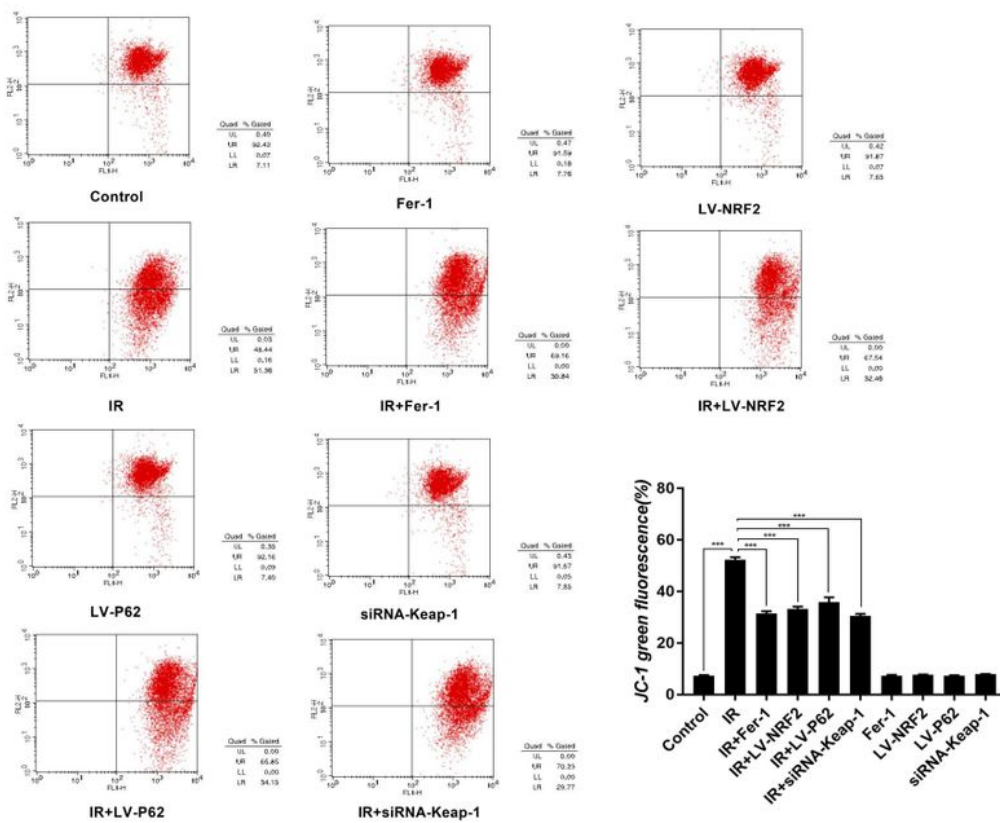
Figure 6

Changes of mitochondrial membrane in different groups. A The morphological changes of mitochondrial membrane in each group were observed by transmission electron microscope. Scale bar: 0.5μm. B Mitochondrial membrane potential in each group with JC-1. (Data shown as mean ± SD, one-way ANOVA followed by a Bonferroni correction, *** P ⪯0.001).

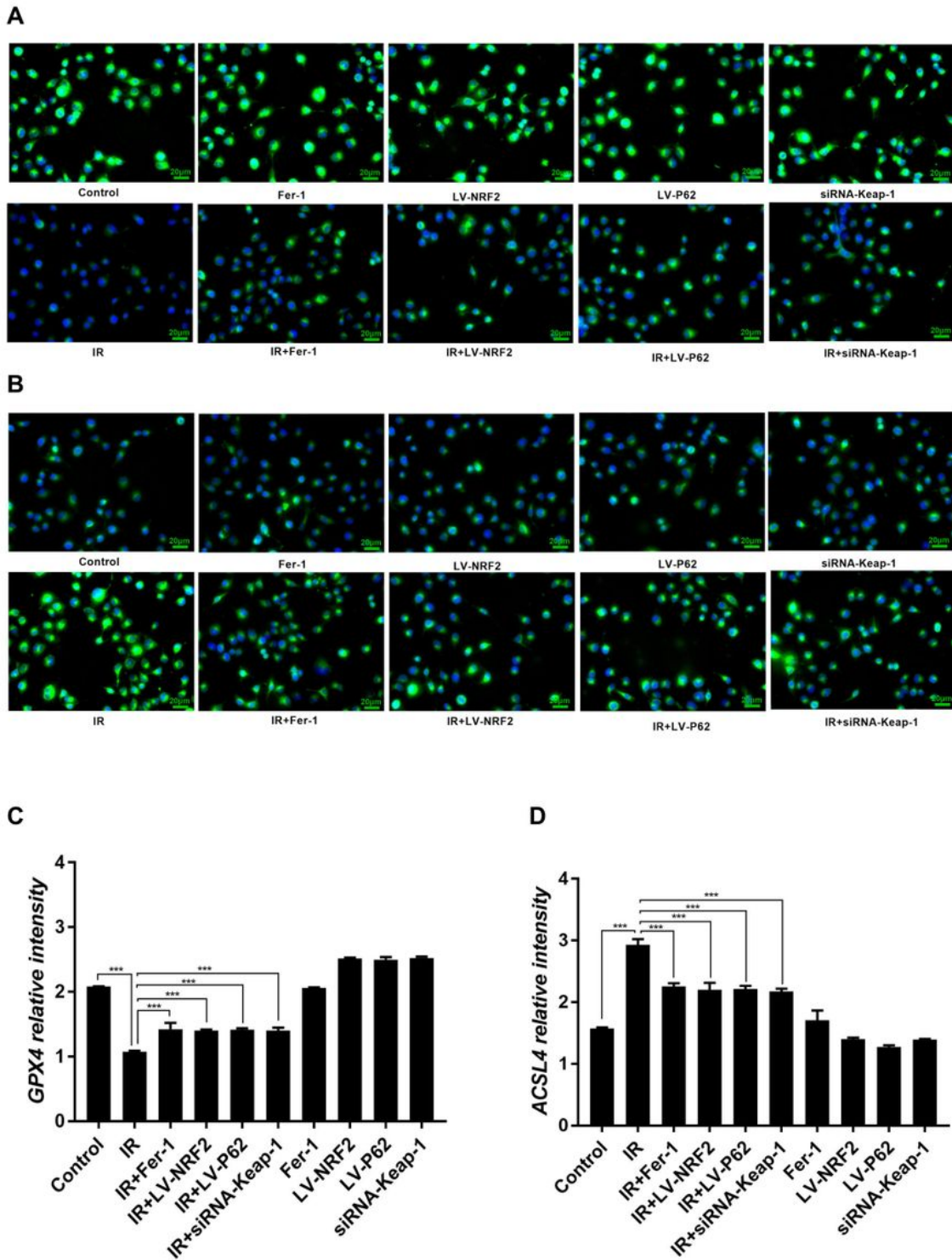**Figure 7**

Expression levels of GPX4 and ACSL4 in cells of each group. A, C Representative fluorescence micrographs of GPX4 staining and Quantification of GPX4 expressions of each group. B, D Representative fluorescence micrographs of ACSL4 staining and Quantification of ACSL4 expressions of each group. (Data shown as mean ± SD, one-way ANOVA followed by a Bonferroni correction, *** P ⩽ 0.001). Scale bar is 20μm.
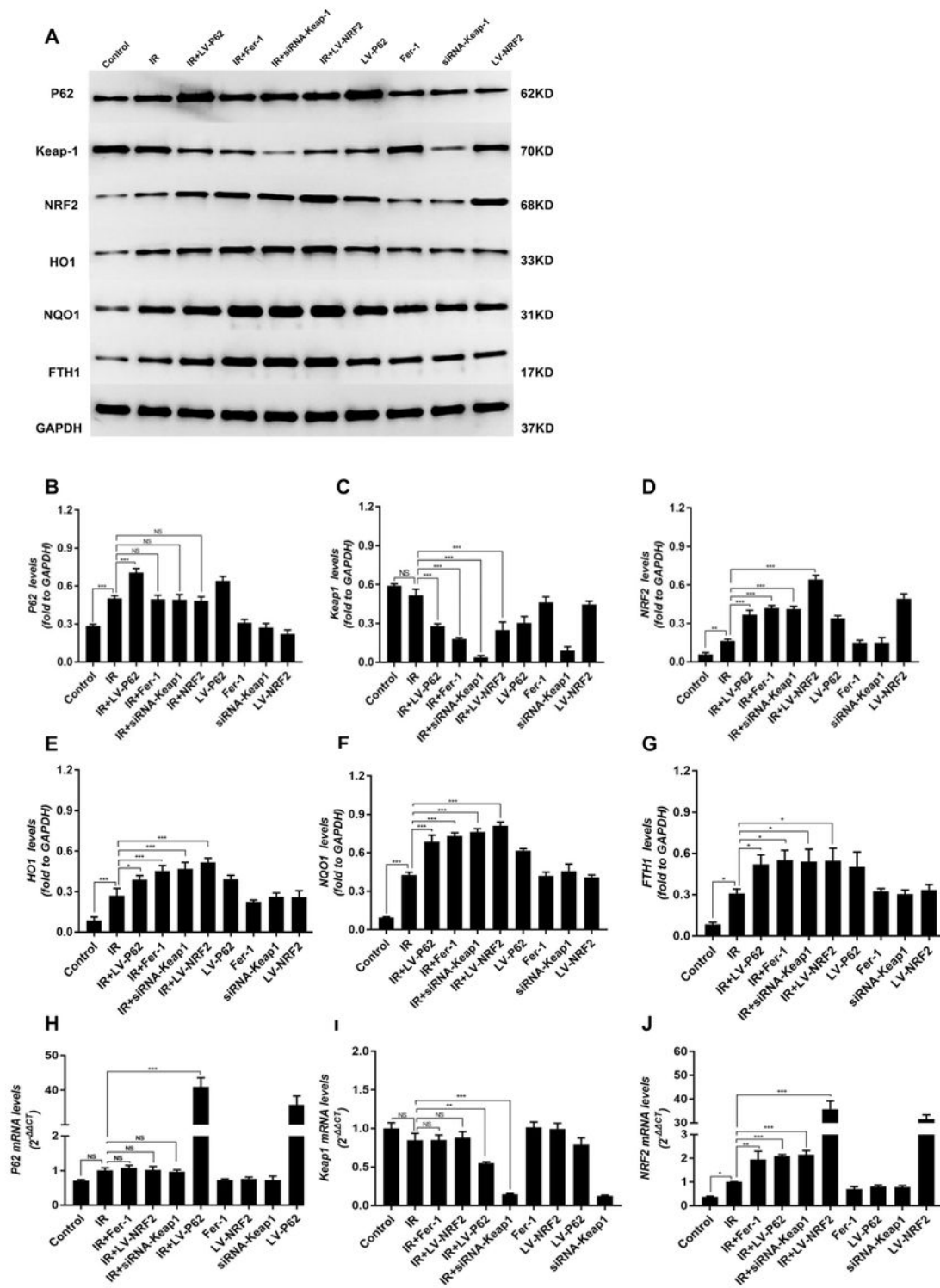
Figure 8

The change of gene expression of P62-Keap1-NRF2 pathway in RILI cells. A, B, C, D, E, F, G The expressions and quantification of P62, Keap1, NRF2, HO1, NQO1 and FTH1 by western blotting. H, I, J The mRNA levels of P62, Keap1 and NRF2 were evaluated by real time PCR. (Data shown as mean ± SD, one-way ANOVA followed by a Bonferroni correction, NS Represented no statistical difference. * P ⊠ 0.05, ** P ⊠ 0.01, *** P ⊠ 0.001).
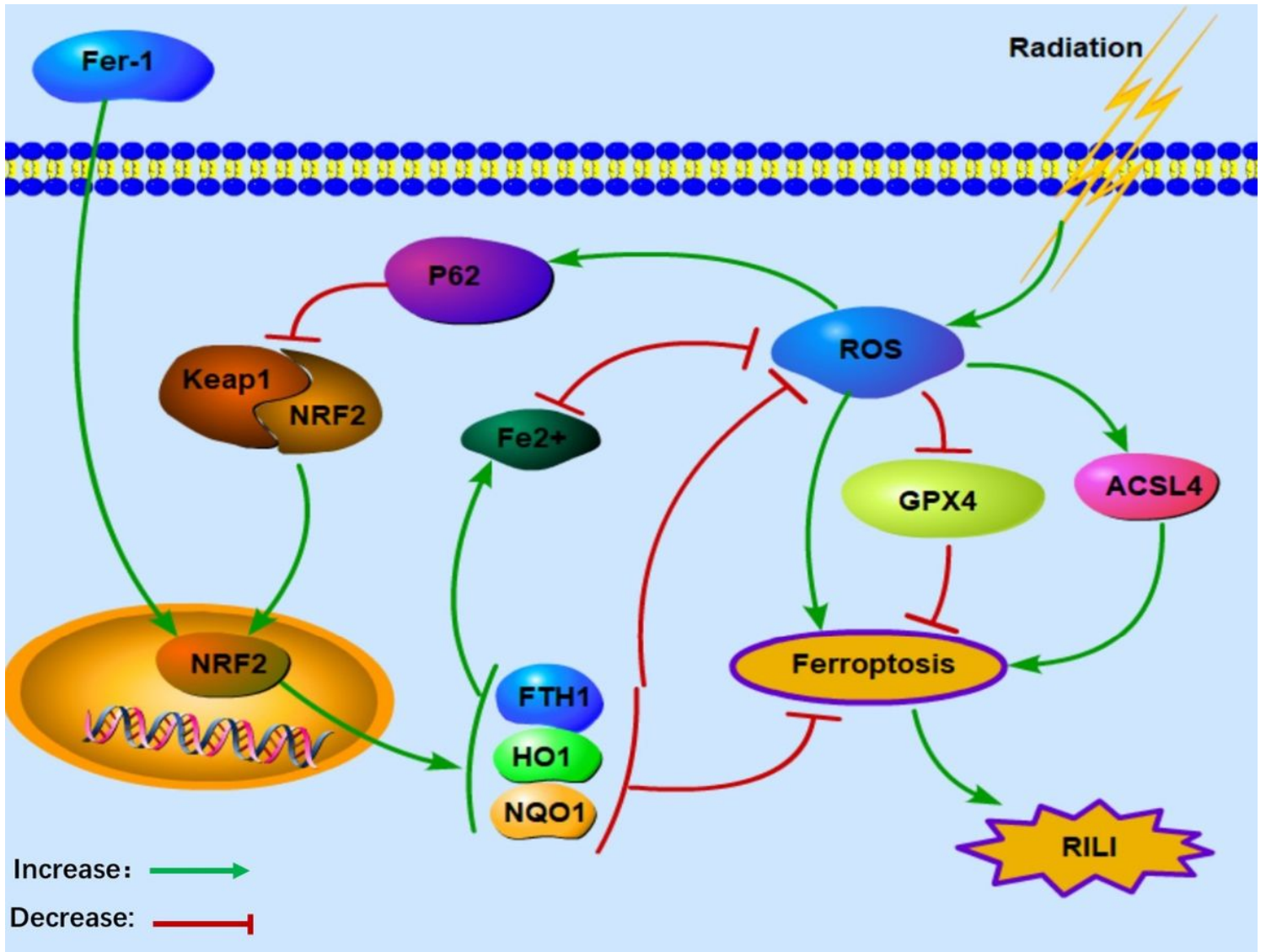
Figure 9

The schematic diagram of P62-Keap1-NRF2 pathway following RILI.